Journal of Advanced Marine Engineering and Technology, Vol. 47, No. 6, pp. 295~302, 2023
J. Advanced Marine Engineering and Technology (JAMET)
https://doi.org/10.5916/jamet.2023.47.6.295

ISSN 2234-7925 (Print)
ISSN 2765-4796 (Online)
**Original Paper**

# Experimental study on the transition to turbulence in secondary acoustic instability in a quarter wavelength resonator

Dae Won Im[1] · Sung Hwan Yoon[†]

(Received December 20, 2023 ; Revised December 21, 2023 ; Accepted December 27, 2023)

**Abstract:** This study explores the intricate dynamics of secondary acoustic instability within a quarter-wavelength resonator, with a specific focus on the interplay between pressure coupling constant ($\beta M$) and flame behavior. Experimental results reveal a strong correlation between key parameters, $\omega_a$(growth rate) and $\omega_d$(decay rate), with $\beta M$, shedding light on the mechanisms governing secondary acoustic instability. The flame thickness reduction, observed as $\beta M$ increases, amplifies the flame front's susceptibility to pressure and temperature perturbations. This heightened sensitivity triggers rapid secondary acoustic instability, characterized by increased $\omega_a$ in the amplification zone. Simultaneously, the absolute value of $\omega_d$ in the damping zone decreases, emphasizing the pivotal role of $\beta M$ in shaping these dynamic behaviors. The observed trends underscore $\beta M$'s significant influence on the growth and decay rates, contributing to a comprehensive understanding of the complex thermos-acoustic phenomena.

**Keywords:** Secondary acoustic instability, Coupling constant, Pressure coupling, Growth rate, Decay rate

## 1. Introduction

In alignment with global initiatives to mitigate greenhouse gas emissions, the International Maritime Organization (IMO) has recently implemented regulations aimed at reducing emissions from maritime vessels by the year 2050 **[1]**. This directive necessitates a global shift in the maritime industry, compelling shipping companies to transition from traditional fossil fuels to more sustainable energy sources, including batteries and hydrogen energy.

In response to these regulatory changes, maritime companies are not only transitioning their primary energy sources from fossil fuels to eco-friendly alternatives but are also innovating in the design of engines and turbines to comply with these new standards. A critical aspect of this innovation process is addressing thermoacoustic instability, a phenomenon known to cause vibration, noise, and potentially severe damage within engine and turbine systems **[2][3][4]**. Effective mitigation of thermoacoustic instability is therefore paramount in the development of next-generation maritime engines and turbines, necessitating a comprehensive understanding of its underlying mechanisms.

Acoustic instability was initially documented by Rayleigh, who elucidated that thermoacoustic instability emerges from a dynamic interaction between heat release and acoustic fluctuations **[5]**. Expanding upon Rayleigh's seminal work, Searby innovatively designed a simplified experimental apparatus to delve deeper into the phenomena of thermoacoustic instability **[6]**. Employing a quarter-wavelength resonator with one open end, Searby conducted controlled experiments using premixed gases, which were ignited at the resonator's upper end. This experimental configuration enabled the observation of a flame propagating downward, exhibiting four distinct behavioral phases:

1. A cellular flame manifesting without acoustic activity post-ignition.
2. The onset of primary acoustic instability characterized by a flat flame surface.
3. The emergence of violent secondary acoustic instability, marked by a corrugated flame structure.
4. The development of a turbulent flame.
5. The initial growth phase of primary acoustic instability, commonly referred to as parametric instability, is typified by a transition from a curved to a flat flame configuration, a change that is accompanied by a linear increase in acoustic pressure **[2][6]**. This primary instability and its associated coupling mechanisms are currently a sub-

† Corresponding Author (ORCID: https://orcid.org/0000-0001-5794-3286): Associate Professor, Department of Marine System Engineering, Korea Maritime & Ocean University, 727, Taejong-ro, Yeongdo-gu, Busan 49112, Korea, E-mail: shy@kmou.ac.kr, Tel: +82-51-410-4261

1 Ph. D. Candidate, Department of Marine System Engineering, Korea Maritime & Ocean University, E-mail: dwim@kmou.ac.kr, Tel: +82-51-410-4261

ject of considerable debate within the scientific community. The prevailing theories are categorized into two main types: acceleration coupling **[7][8][9][10]** and pressure coupling **[2][3][4]**, each vying for recognition as the dominant explanatory model.

In terms of acceleration coupling, it is hypothesized that primary acoustic fields are generated through parametric modulation. This modulation arises from intrinsic flame instabilities, notably the Darrieus-Landau (D-L) instability **[11][12]**, interacting with the standing waves present in the resonator **[7][8][9][10]**. A significant aspect of this theory is that the linear growth rate of pressure is posited to be directly proportional to a coupling constant $(ak)^2$. This constant is defined by the amplitude ($a$) and wavenumber ($k$) of the large curved cells, a phenomenon attributable to the D-L instability.

As for pressure coupling, it focuses on the role of flame thickness, particularly the reaction zone thickness at the juncture of unburned and burned gases within the resonator **[2][3][4]**. Prior research suggests that the pressure growth rate correlates with a coupling constant, which is a product of the Zel'dovich number ($\beta$) and the Mach number ($M$). Zel'dovic number can be calculated as follows:

$$\beta = E\,(T_b - T_u)/(RT_b^2).$$

Here $E$ is the activation energy, $T$ is temperature, and $R$ is the gas constant. The Zel'dovich number, as a nondimensional measure of the reaction rate's sensitivity to temperature variation, implies that acoustic pressure amplification occurs with larger $\beta$ values. In essence, the Zel'dovich number exhibits a tendency to increase in concert with the laminar burning velocity ($S_L$), as the thermal thickness demonstrates an inverse proportionality to $\beta$. Furthermore, acoustic pressure intensity is proportional to this coupling constant. In contrast, the Lewis number ($Le$), representing the ratio of thermal to mass diffusion coefficients, exhibits an inverse relationship with acoustic pressure. It is established that when $Le < 1$, mass diffusion takes precedence, leading to a comparatively thinner flame front that is more responsive to acoustic wave influx **[3]**. Inversely, when $Le > 1$, thermal diffusion becomes more dominant, resulting in a thicker flame front that is less affected by acoustic waves, thereby dampening the effect of acoustic amplification.

Yoon *et al.* recently undertook experimental investigations to validate the correlation between coupling constants as proposed in the theories of acceleration and pressure coupling and their effect on pressure amplification **[2][3]**. Utilizing a $CO_2$ laser, they targeted the unburned gas at the flame front, thereby increasing the local flame velocity through a preheating mechanism. This experimental approach allowed them to manipulate the flame cells, induced by D-L instability, to assess the occurrence of pressure amplification. Contrary to expectations, their findings revealed that pressure amplification was independent of the size of the flame cells. Instead, the extent of pressure amplification was predominantly dictated by the gas composition established at the initial conditions. Most notably, their research provided evidence that the generation of the primary acoustic field is largely governed by pressure coupling. This conclusion was substantiated through the analysis of the pressure coupling constant ($\beta M$) and the corresponding intensity of the acoustic pressure.

This study is committed to the development of parameters for analyzing the coupling mechanisms in secondary acoustic instability occurring within a quarter wavelength resonator, as initially reported by Searby **[6]**. A significant aspect of our research involves conducting experimental validations specifically focusing on pressure coupling within the secondary acoustic instability, with the goal of establishing related parameters. Furthermore, the study aims to conduct a detailed analysis of the interplay between turbulent flames and the secondary acoustic field. Emphasis will be placed on a thorough investigation of the nonlinear acoustic evolution, particularly examining the transition from corrugated structures to turbulent flame states.

## 2. Experimental Method

**Figure 1** illustrates the schematic of the experimental setup utilized in this study. The combustor, designed by Searby **[6]** as an experimental embodiment of the Rayleigh criterion **[5]**, is a transparent quarter-wavelength resonator with an open end. It has dimensions of 3 cm in diameter and 100 cm in height. The composition of the premixed gas was regulated using a mass flow controller (MFC), and the gas was uniformly distributed through a metallic mesh placed at the bottom. **Table 1** details the specific compositions of the premixed gases employed in these experiments. Propane ($C_3H_8$) served as the fuel, with carbon dioxide ($CO_2$) added as a diluent in the basic gas mixture. Flame characteristics such as laminar burning velocities ($S_L$) and adiabatic flame temperatures ($T_b$) were computed using CHEMKIN (Premix code) based on the USC II reaction mechanism **[13]**. Based on the values of $\beta M$, the gas mixtures used in the experiments were classified from Mix.1 to Mix.4.

**Table 1:** Tested gas composition

| Properties / Mixture | $C_3H_8$ [%] | $O_2$ [%] | $CO_2$ [%] | $\Phi$ | $S_L$ [cm/s] | $T_b$ [K] | $Le$ | $\beta M$ |
|---|---|---|---|---|---|---|---|---|
| Mix. 1 | 0.055 | 0.231 | 0.713 | 1.2 | 8.5 | 1882 | 0.77 | 0.0037 |
| Mix. 2 | 0.056 | 0.235 | 0.709 | 1.2 | 9.0 | 1906 | 0.77 | 0.0041 |
| Mix. 3 | 0.048 | 0.240 | 0.712 | 1.0 | 11.5 | 2014 | 0.78 | 0.0050 |
| Mix. 4 | 0.039 | 0.321 | 0.640 | 0.6 | 15.0 | 1854 | 1.52 | 0.0063 |

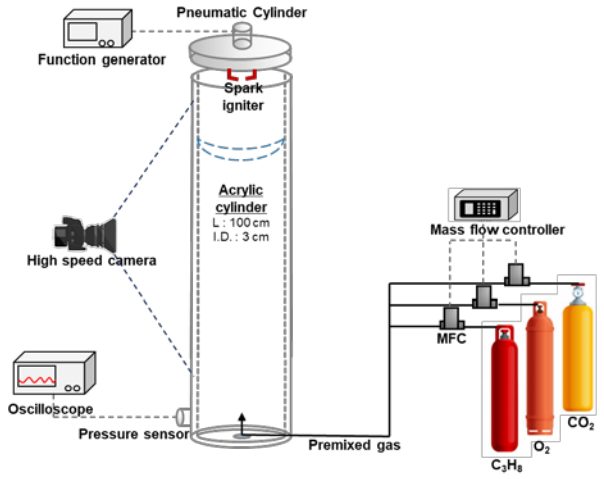


**Figure 1:** Schematic of the experimental equipment setup

The experimental process began by introducing the selected premixed gas into the combustion chamber, initially with the pneumatic cylinder cover open. Subsequently, the cover was closed to allow the system to stabilize for 100 seconds. An automated system, incorporating a pneumatic device and function generator, was employed. Activation of the start button triggered the opening of the cylinder cover via the function generator (Keysight 33400B series), simultaneously igniting the spark. Concurrently, a high-speed camera (Photron Fastcam, SA3) captured the flame's progression starting from a point 3 cm below the top of the tube as the temporal origin (time zero point), spanning a total length of 80 cm, with a resolution of 128 × 1024 pixels at a rate of 500 frames per second (fps). Pressure fluctuations within the combustion chamber were monitored using a dynamic pressure sensor (PCB Piezotronics 106B52) located at the bottom of the tube. An oscilloscope (Tektronix, TBS1102) was used to validate these temporal pressure variations.

## 3. Results and Discussion

### 3.1 Research Target

In this section, we reiterate our study's focus by revisiting Searby's observations **[6]** and clearly defining our research subject. We have performed experimental observations of premixed flames propagating downward in an open-ended tube, adhering to Rayleigh's criterion **[5]**. Typically, a quarter-wavelength resonator exhibits opposing trends in velocity and pressure fields. Our laboratory observations, as depicted in **Figure 2**, have captured the process of thermoacoustic instability within such a resonator. Post-ignition, at the apex of the resonator, curved flames manifest hydrodynamic instability (or D-L, instability) with no detectable acoustic pressure. Midway down the tube, the emergence of a flat flame, resonating at a frequency marginally above the fundamental, is accompanied by the onset of nominal acoustic pressure. This frequency elevation is attributable to the accelerated sound speed within the resonator, a consequence of the hot gases produced during combustion. Following this phase, acoustic pressure stabilizes, sustaining the vibrating flat flame, indicative of primary acoustic instability. This is succeeded by a marked surge in acoustic pressure, coinciding with the formation of a corrugated flame surface—a hallmark of secondary instability. Such a phenomenon is exclusive to high laminar burning velocities and bears resemblance to Faraday instability. A pronounced vibration amplitude persists over 5-10 cycles before the flame transitions into a turbulent state, whereupon acoustic pressure sharply declines. This pattern consistently ensues post-secondary acoustic instability. It is pivotal to note that our study concentrates on elucidating the transition from secondary acoustic instability to turbulence.

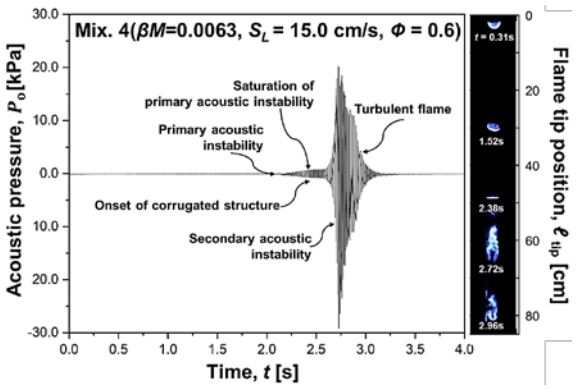


**Figure 2:** Acoustic pressure at the bottom of the tube with sequential images for a propagating flame at Mix. 4

### 3.2 Dynamic Flame Behaviors in Parametric Instability

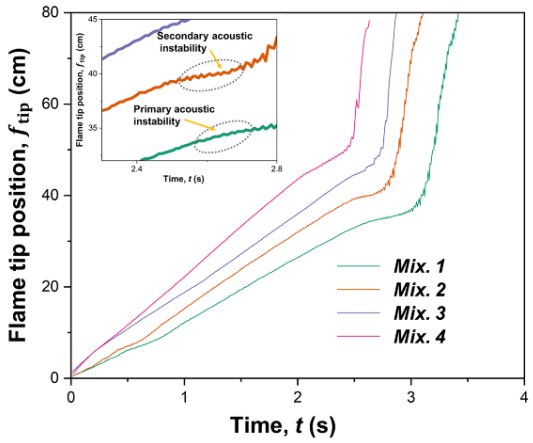


**Figure 3:** Comparative analysis of flame tip position versus time for different gas mixtures Indicating primary and secondary acoustic instability regions

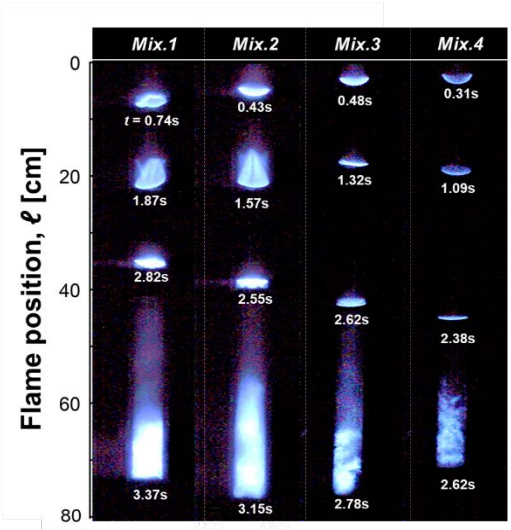


**Figure 4:** Sequential flame images demonstrating the propagation distance over time for various gas mixtures, corresponding to temporal flame tip positions in **Figure 3**

**Figure 3** illustrates the time-dependent progression of the flame tip position. The flame advances at a uniform velocity until it reaches a specific juncture (roughly 30 to 50 cm from the resonator's apex), at which a distinct acceleration is observable. Complementary to **Figure 3**, **Figure 4** displays a chronological array of flame images for various gas mixtures. For Mix. 1, which exhibits the lowest $S_L$ and $\beta M$ values, the flame's displacement speed ($S_d$) in the non-acoustic field emanating from the resonator's top is calculated to be 13.51, which is marginally higher than the actual $S_L$ (8.5 cm/s). This increment is likely due to an increased flame surface area, a consequence of the D-L instability. An augmentation in flame surface area is evident at 1.30 seconds for Mix. 1 as depicted in **Figure 4**. A similar pattern is noted for other mixtures, with the $S_d$ for Mix. 2 through 4 recorded at 17.14, 16.57, and 21.98 cm/s, respectively. These values represent a greater than 50% enhancement in $S_d$ relative to $S_L$, a phenomenon previously attributed to the gas expansion effect stemming from density disparities between unburned and burned gases **[11][12]**. There is no measured acoustic frequency because the flame does not vibrate in this region.

Moving on to the primary acoustic field, it can be observed for Mix. 1 between approximately 1.55 and 1.90 seconds, where the vibrating flat flame is a dominant feature (refer to **Figure 4** at $t$ = 1.62 s for Mix. 1). During this phase, $S_d$ for Mix. 1 is measured at 8.73 cm/s, slightly lower than in the non-acoustic field, and approximates the $S_L$. This trend is consistent across the other mixtures, with $S_d$ for Mix. 2 through 4 sequentially measured at 10.03, 14.60, and 15.42 cm/s, indicating values close to the $S_L$.

This suggests that the inherent instability of the flame, namely the D-L instability, is suppressed in the primary acoustic region, thus excluding the effect of flame curvature. Consequently, the values obtained are very similar to the theoretical flame propagation velocity. To elucidate this point further, **Figure 5** presents the variation of $S_d$ with $S_L$ in the primary acoustic field.

As depicted, a linear relationship can be discerned, and the slope (= 1.01) of the fitting function is noted to be nearly 1, with a correlation coefficient of 0.84.

$$S_d = 1.01 \cdot S_L + 0.95. \qquad (R = 0.84)$$

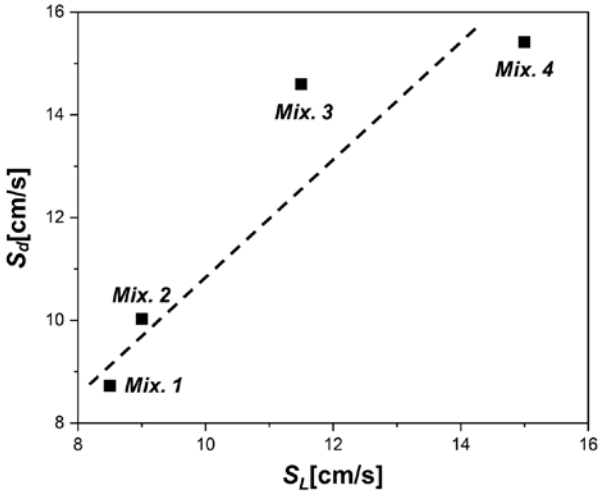


**Figure 5:** Displacement flame velocity ($S_d$) as a function of laminar burning velocity ($S_L$) in the primary acoustic field

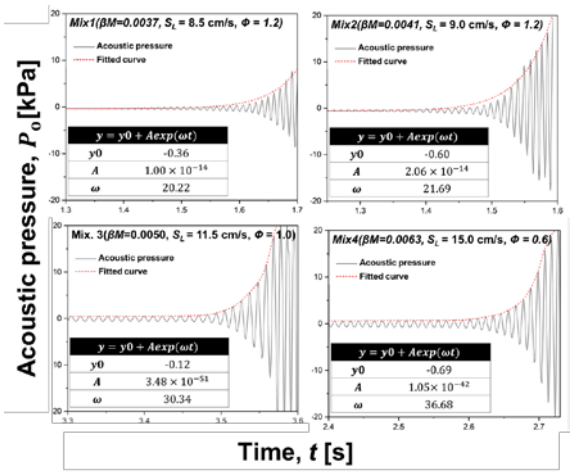


**Figure 6:** Grow rate of acoustic pressure in secondary acoustic instability with various gas mixtures

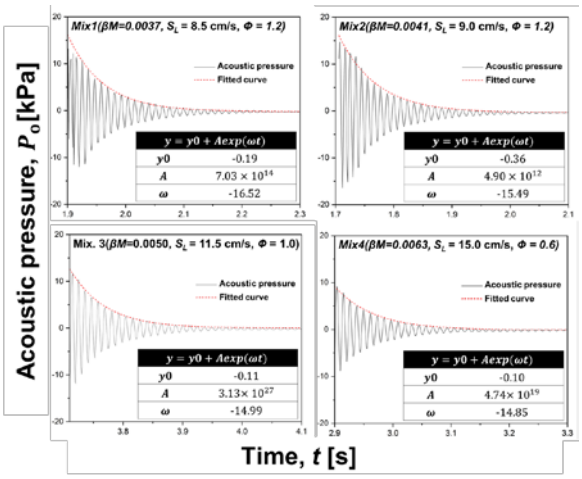


**Figure 7**: Decay rate of acoustic pressure in turbulization with various gas mixtures

In analyzing the acoustic frequency trends within the primary acoustic field, the frequencies for Mix. 1 through 4 were determined to be 91.95, 85.79, 85.98, and 85.84 Hz, respectively. These values are found to be very similar to the fundamental frequency, which is assumed to be 85 Hz for the speed of sound in air. Thus, it is evident that the acoustic frequencies in the primary acoustic field do not deviate from the fundamental frequency.

In examining the secondary acoustic field, the case of Mix. 1 can be observed between approximately 2.60 and 3.00 seconds, with a prominent characteristic being the formation of a corrugated structure on the flame surface. During this interval, $S_d$ of Mix. 1 is noted to be 6.85 cm/s, which is the lowest when compared to both the non-acoustic and primary acoustic fields. A similar pattern is evident in other mixtures as well, where Mix. 2 through 4 exhibit $S_d$ values of 5.65, 10.19, and 14.37 cm/s, respectively. These values represent the slowest flame velocities encountered during the flame's propagation within the resonator. It is crucial to understand that in this context, $S_d$ refers to the average value of displacement flame velocity, not the instantaneous velocity during vibrations, and this average value of displacement flame velocity indicates a non-zero average displacement. Within the secondary acoustic field, the flame experiences 5-10 cycles of high amplitude vibrations before it transitions seamlessly into a turbulent flame.

In our examination of the secondary acoustic field, we focused on evaluating the growth rate of acoustic pressure. **Figure 6** displays the time-dependent acoustic pressure for each of the gas compositions we selected.

The figure clearly shows that the acoustic pressure in each case undergoes exponential and explosive amplification over time. To conduct a quantitative analysis of the growth rate in this phase of amplification, we applied curve fitting using an exponential function to the crest of the acoustic fluctuations. The equation used for the curve fitting is as follows:

$$P_{crest} = Y_0 + A \cdot e^{\omega t}.$$

Here, the parameter $\omega$, which denotes the slope of the growth rate is listed in the accompanying table for each figure. $Y_0$ and $A$ are disregarded since they do not influence the grow rate but only impact the acoustic value itself. Notably, an increase in $S_L$ or $\beta M$ correlates with an increase in $\omega$, suggesting that, as with the primary acoustic field found in previous studies **[2]**, pressure coupling plays a crucial role in the growth rate of pressure waves during secondary acoustic instability.

Further analysis of acoustic frequency trends within the secondary acoustic field revealed values of 100.53, 110.53, 91.60, and 94.24 Hz for Mix. 1 through 4, respectively. These frequencies are 5-10 Hz higher compared to those in the primary acoustic field, which can be attributed to the expanded volume occupied by the burned gases within the resonator. This expansion leads to an increase in the speed of sound in the fluid, impacting the acoustic frequency.

Turning our attention to turbulent flames, let's start with Mix 1. As evidenced in **Figure 3**, the onset of turbulence is marked by a notable surge in $S_d$. Complementary to this, **Figure 4** illustrates a rapid, explosive expansion in the flame's surface area, accompanied by the formation of characteristic eddies indicative of turbulent flames. In the case of Mix 1, $S_d$ peaks at 151.07 cm/s, the highest velocity observed across all acoustic development

stages. This high velocity trend is consistent across other mixtures as well, with Mix 2 to 4 showing $S_d$ values of 139.95, 210.66, and 190.39 cm/s, respectively. These values represent the highest flame speeds during propagation within the resonator. Post the turbulent phase, the flame exhausts all the premixed gas in the resonator, leading to its natural extinction.

Furthermore, our study evaluates the acoustic decay rate in the damping zone of the turbulent flame. **Figure 7** depicts the acoustic pressure over time for each gas mixture, revealing a uniform pattern of exponential and rapid decay in acoustic pressure across all mixtures.

To quantify the decay rate in this damping phase, we employed exponential curve fitting on the crest of acoustic fluctuations. The calculated decay slope, represented by $\omega$, is included in the table accompanying each figure. Intriguingly, an increase in $S_L$ or $\beta M$ results in a decrease in the absolute value of $\omega$. This observation aligns with the shift in the relative position of secondary instability occurrence within the resonator, as shown in **Figure 3**. Specifically, a higher $S_L$ or $\beta M$ correlates with an upward shift in the onset of secondary instability. This shift suggests a shorter residence time for the turbulent flame. Further analysis of acoustic frequency trends within the turbulent revealed values of 129.0, 110.2, 125.5, and 114.2 Hz for Mix. 1 through 4, respectively Consequently, it is inferred that an increase in $S_L$ or $\beta M$, which leads to a thinner flame thickness, precipitates an earlier occurrence of secondary instability, resulting in a diminished absolute value of the acoustic decay rate in the damping zone of the turbulent flame.

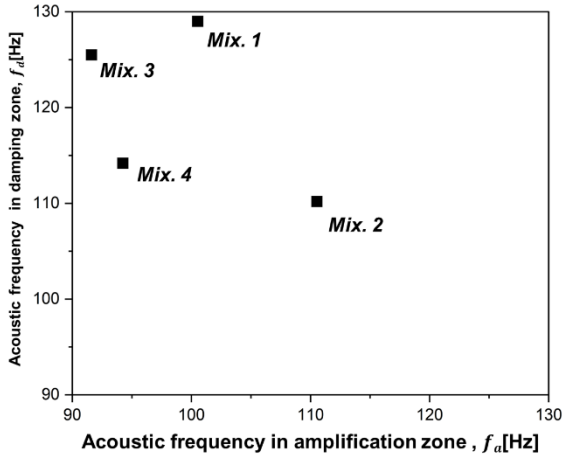


**Figure 8**: Acoustic frequency in damping zone ($f_d$) as a function of Acoustic frequency in amplification zone ($f_a$) with various gas mixtures

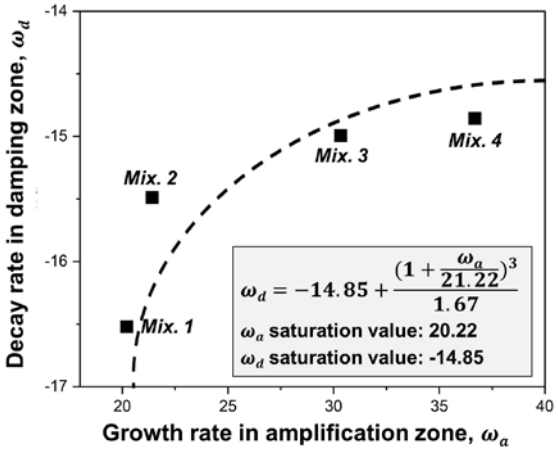


**Figure 9:** Decay rate ($\omega_d$) in damping zone as a function of grow rate ($\omega_a$) in amplification zone with various gas mixtures

**Figure 8** depicts the relationship of frequency in amplification zone ($f_a$) to acoustic frequency in damping zone ($f_d$) for various gas mixtures. It is observed that the acoustic frequency increases relatively in the damping zone of the flame. This can be attributed to the increase in heat release as the flame surface and velocity increase, acting as a scattering factor for the frequency.

Now, our focus shifts to analyzing the correlation between $\omega_a$ and $\omega_d$ in the amplification and damping zones, as derived from our experimental results. **Figure 9** depicts the relationship of $\omega_a$ to $\omega_d$ for various gas mixtures we have utilized.

To quantitatively analyze this relationship, we employed logistic regression analysis, one of the predictive models that also gives information about saturation, and fitted the data to the following equation:

$$\omega_d = -14.85 + \frac{\left(1+\frac{\omega_a}{21.22}\right)^3}{1.67}.$$

As seen in **Figure 9**, in the amplification zone, an increase in $\omega_a$ leads to a decrease in the absolute value of $\omega_d$, eventually reaching saturation at a specific value.

Additionally, an increase in the absolute value of $\omega_d$ in the damping zone correlates with a saturation of $\omega_a$ in the amplification zone. Utilizing extrapolation methods, the saturation values were determined as $\omega_a$ = 20.22 and $\omega_d$ = -14.85. It's important to reiterate that a high $\omega_a$ in the amplification zone physically signifies that the coupling strength between the flame and the acoustic field exceeds a critical threshold, leading to a rapid onset of nonlinear instability. This implies an earlier occurrence of secondary acoustic fields, which, in turn, increases the resi-

dence time of turbulent flames within the resonator. Consequently, we can infer that the increased residence time of turbulent flames in a confined space leads to a decrease in $\omega_d$.

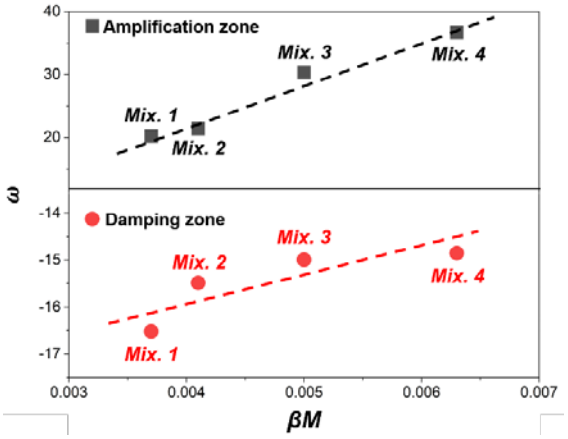


**Figure 10:** Dependence of growth rate ($\omega$) in amplification and damping zone on $\beta M$ values with various gas mixtures

Lastly, to confirm the close relationship between the growth mechanism of secondary acoustic instability and pressure coupling, **Figure 10** illustrates the correlation between $\omega_a$ and $\omega_d$ with the pressure coupling constant, $\beta M$. As evident in the figure, both $\omega_a$ and $\omega_d$ exhibit a linear relationship with $\beta M$. Below are the fitting functions and their respective correlation coefficients:

$$\omega_a = 6665.79 \cdot \beta M - 4.67, \qquad (R = 0.97)$$
$$\omega_d = 548.26 \cdot \beta M - 18.08. \qquad (R = 0.71)$$

In essence, as $\beta M$ increases, the flame thickness diminishes, making the flame front more susceptible to pressure and temperature fluctuations. Subsequently, when the coupling strength between the flame and the acoustic field surpasses a critical threshold, it triggers rapid growth in secondary acoustic instability. Consequently, $\omega_a$ of the acoustic field increases, and due to this heightened $\omega_a$, $\omega_d$ (in absolute terms) of the turbulent flame decreases.

## 4. Conclusion

This study has rigorously investigated the mechanisms of secondary acoustic instability within a quarter-wavelength resonator, focusing on the interplay between pressure coupling and the dynamic behaviors of flames. Our findings highlight the critical role of the pressure coupling constant, $\beta M$, in influencing the characteristics of flame behavior and acoustic pressure variations.

We observed that the flame thickness reduces as $\beta M$ increases, enhancing the flame front's sensitivity to pressure and temperature perturbations. This sensitivity is a key factor in the rapid onset of secondary acoustic instability. Our experiments revealed a direct correlation between the growth rate ($\omega_a$) in the amplification zone and the decay rate ($\omega_d$) in the damping zone of turbulent flames. Specifically, an increase in $\omega_a$ correlates with a decrease in the absolute value of $\omega_d$, underscoring the influence of $\beta M$ on these parameters.

Furthermore, the study has successfully demonstrated the linear relationship between the growth and decay rates with βM, providing significant insights into the mechanisms governing secondary acoustic instability.

In summary, our research offers a comprehensive understanding of the complex dynamics involved in secondary acoustic instability. The insights gained from this study are not only pivotal in advancing the theoretical understanding of thermos-acoustic phenomena but also have practical implications for the design and development of more efficient and stable engines and turbines in the maritime industry. The findings of this study pave the way for further research and development in this field, with the potential to significantly enhance the operational safety and efficiency of maritime propulsion systems.

## Acknowledgements

This research was supported by Basic Science Research Program through the National Research Foundation of Korea (NRF) funded by the Ministry of Education (No. 2021R1I1A3061305).

## Author Contributions

Conceptualization, D. W. IM and S. H. YOON; Methodology, D. W. IM; Software, D. W. IM; Validation, D. W. IMand S. H. YOON; Formal Analysis, D. W. IM; Investigation, D. W. IM; Resources, S. H. YOON; Data Curation, D. W. IM; Writing—Original Draft Preparation, D. W. IM; Writing—Review & Editing, S. H. YOON; Visualization, D. W. IM; Supervision, S. H. YOON; Project Administration, S. H. YOON; Funding Acquisition, S. H. YOON

## References

[1] IMO, Initial IMO strategy on reduction of GHG emission from ships, MEPC 72/17/Add. 1 Annex 11, p. 1, International Maritime Organization: London, April 16, 2018.

[2] S. H. Yoon, T. J. Noh, and O. Fujita, “Onset mechanism of primary acoustic instability in downward-propagating flames,” Combustion and Flame, vol. 170, pp. 1-11, 2016.

[3] S. H. Yoon, T. J. Noh, and O. Fujita, “Effects of Lewis number on generation of primary acoustic instability in downward-propagating flames,” Proceedings of the Combustion Institute, vol. 36, no. 1, pp. 1603-1611, 2017.

A. K. Dubey, Y. Koyama, S. H. Yoon, N. Hashimoto, and O. Fujita, “Range of “complete” instability of flat flames propagating downward in the acoustic field in combustion tube: Lewis number effect,” Combustion and Flame, vol. 216, pp. 326-337, 2020.

[4] J. Rayleigh, “The explanation of certain acoustical phenomena,” Nature, vol. 18, pp. 319-321, 1878.

[5] G. Searby, “Acoustic instability in premixed flames,” Combustion Science Technology, vol. 81, no. 4-6, pp. 221-231, 1992.

[6] G. H. Markstein, “Flames as amplifiers of fluid mechanical disturbances,” Proceedings of the 6th National Congress for Applied Mechanics, Cambridge, MA, pp. 11-33, 1970.

[7] P. Pelcé and D. Rochwerger, “Vibratory instability of cellular flames propagating in tubes,” Journal of Fluid Mechanics, vol. 239, pp. 293-307, 1992.

[8] G. Searby and D. Rochwerger, “A parametric acoustic instability in premixed flames,” Journal of Fluid Mechanics, vol. 231, pp. 529–543, 1991.

[9] C. Clanet, G. Searby, and P. Clavin, “Primary acoustic instability of flames propagating in tubes: cases of spray and premixed gas combustion,” Journal of Fluid Mechanics, vol. 385, pp. 157-197, 1999.

[10] G. Darrieus, “Propagation d’un front de flamme. Unpublished work presented,” La Technique Moderne and at Le Congrés de Mécanique Appliqueée, 1938.

[11] L. Landau, “On the theory of slow combustion,” Acta Physicochimica URSS, vol. 19, pp. 77-85, 1944.

[12] R. J. Kee, R.M. Rupley, J. A. Miller, Sandia National Laboratories: Albuquerque, NM, SAND 89-8009B, 1989.